Title: RNA Polymerase II-mediated transcription is required for repair of ribosomal DNA breaks in nucleolar caps, guarding against genomic instability

- **Short Title: RNAPII promotes ribosomal DNA stability**

Authors

Cintia Checa-Rodríguez[1,7], Beatriz Suárez-Quintero[1,2,7], Laura Contreras[1,2], Lea Korsholm[3], Dorthe Helena Payne-Larsen[3], Jesús de la Cruz[1,2], Jiri Bartek[4,5], Daniel Gómez-Cabello[1,6*].

Affiliations

1. Instituto de Biomedicina de Sevilla (IBiS), Hospital Universitario Virgen del Rocío/CSIC/Universidad de Sevilla, 41013 Seville, Spain.
2. Departamento de Genética, Facultad de Biología, Universidad de Sevilla, 41012 Seville, Spain.
3. Nucleolar Stress and Disease Group, Danish Cancer Society Research Center, Strandboulevarden 49, Copenhagen, DK-2100, Denmark.
4. Genome Integrity Group, Danish Cancer Society Research Center, Strandboulevarden 49, Copenhagen, DK-2100, Denmark.
5. Division of Genome Biology, Department of Medical Biochemistry and Biophysics, Science for Life Laboratory, Karolinska Institute, Scheele's vag 2, Stockholm, 17177, Sweden.
6. Departamento de Biología Celular, Facultad de Biología, Universidad de Sevilla, 41012 Seville, Spain.
7. These authors contributed equally.

**Corresponding author. Email: dgcabello@us.es*

Abstract

Ribosomal DNA (rDNA) double-strand breaks (DSBs) threaten genome integrity due to the repetitive and transcriptionally active nature of rDNA. The nucleolus, while central to ribosome biogenesis, also functions as stress sensor. Here, we identify a transcription-dependent mechanism in which RNA polymerase II (RNAPII) is essential for homologous recombination (HR) repair of rDNA DSBs. Using CRISPR-induced breaks, high-resolution imaging, and transcriptional inhibition, we show that RNAPII activity drives the formation of nucleolar repair caps. Mechanistically, CtIP promotes RNAPII recruitment and H3K36 trimethylation at rDNA lesions, facilitating HR. Disruption of this RNAPII–CtIP–H3K36me3 axis impairs cap formation and repair, leading to persistent damage. RNAPII inhibition exacerbates genome instability and synergizes with rDNA breaks to induce cancer cell death, without acutely impairing ribosome function. These findings uncover a co-transcriptional mechanism of rDNA repair and highlight RNAPII-mediated chromatin remodeling and spatial reorganization as key to nucleolar genome maintenance and potential targets for cancer therapy.

Teaser (one sentence, max125 char./= short abstract)

Nascent RNA synthesis by RNAPII safeguards ribosomal DNA integrity to avoid genomic instability in human cells.

Graphical Abstract

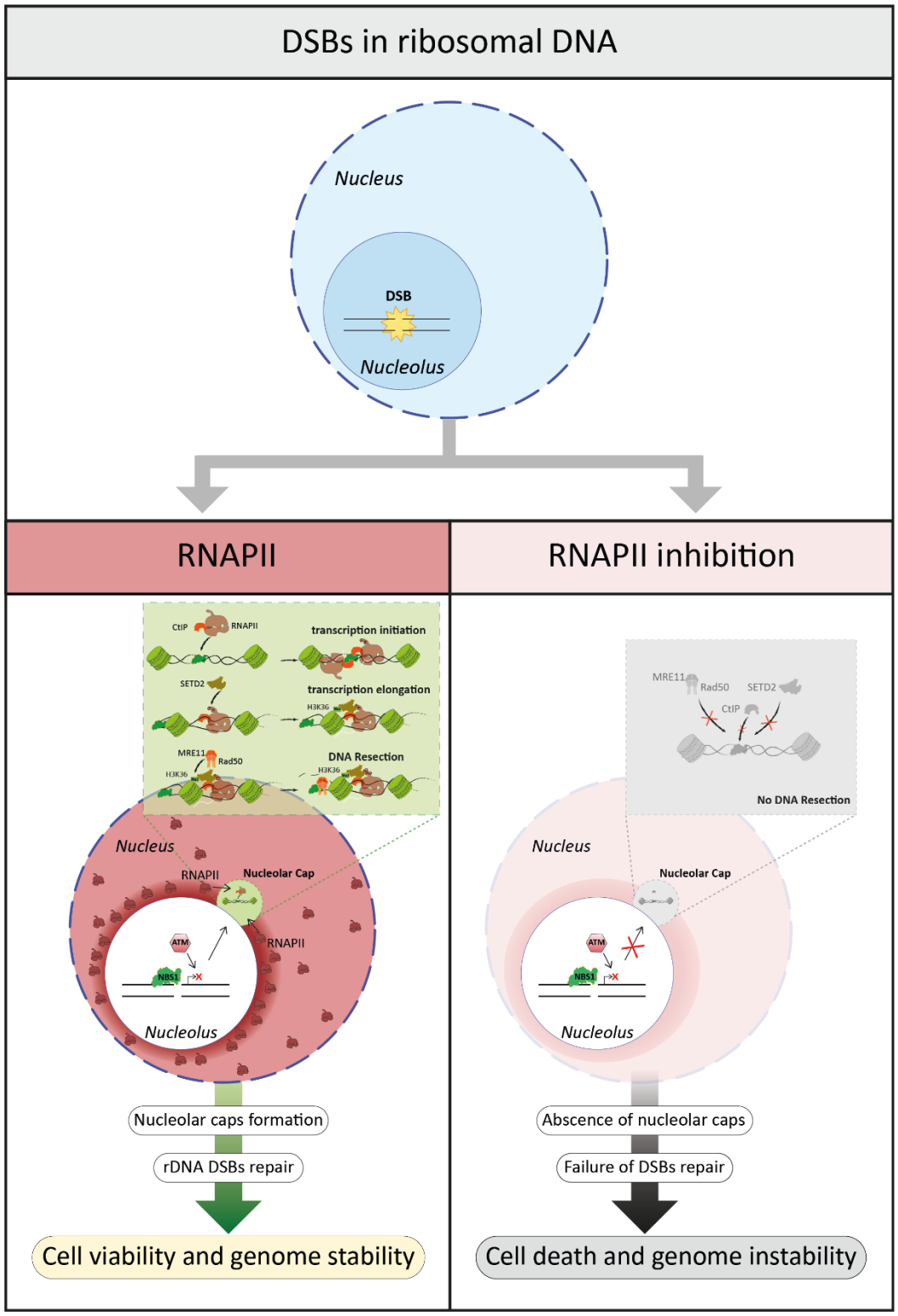

MAIN TEXT

Introduction

The nucleolus is a cellular sensor for diverse exogenous and intracellular insults. The nucleolus is a membrane-less intranuclear organelle whose canonical function is ribosome biogenesis (RiBi). RiBi includes ribosomal DNA (rDNA) transcription, rRNA processing and assembly of ribosomal subunits that are orchestrated in a complex multistep process leading to ribosome formation [1]. Enlarged nucleoli due to elevated protein synthesis and cell metabolism, including RiBi, adapted to cope with aberrant growth and proliferation, is one of the long-established hallmarks of cancer cells [2]. The nucleolus is also considered a central response hub for the stressors that promote cancer development [3]. The study of nucleolar stress has been motivated, among other reasons, by efforts to interfere with RiBi function or inhibit RNA polymerase I (RNAPI), the enzyme responsible for transcription of rDNA, as strategies for cancer treatment in both preclinical and clinical settings[4].
The human genome contains around 200-600 tandem repeats of 28S, 18S and 5.8S rDNA genes dispersed in chromosomes 13, 14, 15, 21 and 22. The active rDNA sequences are concentrated in the nucleolar organizer regions (NORs), which are prone to replication-transcription conflicts potentially leading to genome instability [5]. Such conflicts occur mainly because RNAPI-mediated transcription represents almost 60% of the total cellular transcription in eukaryotic cells [6, 7]. The occurrence of such hazardous transcription-replication conflicts is enhanced in tumor cells which show both aberrantly elevated rDNA transcription and deregulated genome replication as common features of oncogenic transformation [8-10]. Due to such 'nucleolar stress', rDNA instability occurs commonly during tumorigenesis, likely fueling tumor progression due to rDNA rearrangements events including insertions, translocations and amplifications [11]. Among the different rDNA lesions arising from transcription-replication conflicts, the rDNA double-strand breaks (rDNA DSBs) are arguably the most cytotoxic and difficult to repair type of DNA damage [12-14]. The two main pathways for DSB repair are homologous recombination (HR) and non-homologous end joining (NHEJ), both of which contribute to rDNA stability upon oncogenic or genotoxic stresses, such as activated cMYC oncogene and ionizing radiation (IR), respectively [14, 15]. The NHEJ process involves little if any DNA end processing and is potentially mutagenic. On the other hand, the HR pathway is a more precise DSB repair mechanism that avoids loss of genetic information, due to faithful repair based on using a homologous DNA sequence as a template [13, 16]. However, the HR machinery is largely absent from the nucleolar inside since intra-nucleolar recombination processes would induce illegitimate rearrangements among the many rDNA repeats localized on different chromosomes, with catastrophic consequences for the cell [17].

92 Key elements of the complex spatio-temporal cascade of DNA damage signaling and repair factors
93 in response to rDNA lesions remain poorly understood. Recently, it has been shown that upon
94 rDNA DSB formation, ATM-TCOF interplay promotes transient transcriptional inhibition of
95 RNAPI and rDNA relocalization into newly formed structures at the nucleolar periphery, known as
96 nucleolar caps [18-20]. However, the roles of various HR factors in rDNA repair appear to be
97 controversial, depending on the type of DSB-inducing insult, for example, IR *versus* the
98 enzymatically induced DNA breaks [21]. Indeed, HR factors such as RAD51 contribute to rDNA
99 repair but their accumulation in the absence of the BLM protein, increases genome instability[22] .
100 Moreover, it has not yet been established what determines relocation of some rDNA DSBs to the
101 nucleolar periphery for their HR-mediated repair, in so-called Nucleolar caps.
102 Recently, we and others have demonstrated the essential role of RNA polymerase II (RNAPII) and
103 RNA polymerase III (RNAPIII) in the cell's choice of DSB repair by HR rather than NHEJ in the
104 whole genome. This decision is facilitated by transcription of nascent RNA flanking the DSB sites,
105 as an early and pivotal[12, 23, 24]. Although the crosstalk between transcription and DSB repair is well
106 established, it remains controversial whether RNAPII[25-27] or whether its presence is limited to
107 transcriptionally active regions, where RNA:DNA hybrids form as a consequence of ongoing
108 transcription[28-30]. Furthermore, generally RNAPII inhibition impairs recruitment of HR factors to
109 DSBs, mainly by preventing the early steps of CtIP[12].
110 Notably, the molecular signals and mechanisms driving the nucleolar cap formation and HR
111 engagement in repair of rDNA DSBs remain poorly defined. Until recently RNAPII was not
112 thought to play a role in the nucleolus but it has been shown to be an important regulator of RNAPI
113 transcription[31, 32]. More recently genotoxic stress was shown to induce RNAPII dependent
114 transcription of the intergenic spacer region in rDNA sequestering aberrant transcripts to promote
115 DNA repair[33]. However, if RNAPII plays a role in regulation of the specialized nucleolar DNA
116 Damage Response (nDDR) remains unexplored. This raises the possibility that RNAPII may be
117 locally co-opted to support rDNA repair, particularly through its transcription-coupled chromatin
118 remodeling functions.
119 Here, we demonstrate that RNAPII activity is essential for the accurate repair of rDNA DSBs via
120 HR. Using CRISPR-based targeted rDNA DSBs, transcriptional inhibition, high-resolution
121 imaging, and chromatin profiling, we uncover a transcription-dependent mechanism in which
122 RNAPII, together with the DNA end-resection factor CtIP and the H3K36me3 histone marker,
123 orchestrate the recruitment of some DNA resection factors to rDNA lesions. RNAPII inhibition
124 disrupts nucleolar cap formation, impairs DNA end resection and induces genome instability and
125 cell death. Mechanistically, CtIP enables RNAPII recruitment and transcriptional activation at
126 rDNA breaks, allowing deposition of H3K36me3, a histone mark crucial for HR engagement.

Our findings reveal a previously unrecognized transcription-coupled repair program within nucleolar chromatin. We propose that a CtIP–RNAPII–H3K36me3 axis facilitates rDNA break relocation, transcriptional activation, and chromatin remodeling to enable HR at nucleolar caps. This mechanism underscores the importance of RNA-mediated genome surveillance in ribosomal DNA maintenance and highlights novel vulnerabilities that could be exploited in cancer therapy.

Results

Role of RNAPI, RNAPII and RNAPIII in rDNA repair.

To investigate the mechanisms underlying the role of RNAPs in rDNA repair within nucleolar caps, we first selectively inhibited RNAPI, RNAPII, and RNAPIII. We took advantage of our well-characterized human sarcoma U2OS-based cell model that stably expresses the endonuclease Cas9 and a GFP-tagged version of the DDR protein NBS1 [11, 22, 34]. Following transfection with three guide RNA vectors targeting the 5´ETS region and intergenic regions of rDNA (Fig. 1a, left), DNA repair-associated nucleolar caps formed at the nucleolar periphery within six hours (Fig.1a, right). To evaluate the impact of RNAP inhibition, cells were treated with the different inhibitors for two hours prior to fixation at the six-hour time point. Notably, the nucleolar caps associated with rDNA repair examined in this study differ from those induced by RNAPI inhibitors such as actinomycin D, BMH-21, and CX5461, which show complete absence of NBS1 (Fig. S1). To specifically investigate the role of RNAPs in rDNA damage repair—and to avoid analyzing nucleolar caps not associated with DNA repair—we focused exclusively on NBS1-positive nucleolar caps (Fig. S1). For subsequent experiments, we used BMH-21 to inhibit RNAPI, THZ1—a covalent CDK7 inhibitor previously shown to impair HR genome-wide—to inhibit RNAPII, and ML-60218 as an RNAPIII inhibitor. We observed that the proportion of cells displaying more than one NBS1-positive nucleolar cap was unaffected by BMH-21 or ML-6021, whereas treatment with the RNAPII inhibitor THZ1 led to a greater than two-fold reduction in nucleolar cap formation at the nucleolar periphery (Fig. 1b). THZ1 also significantly decreased both the average number and distribution of nucleolar caps per cell, an effect not observed upon either RNAPI or RNAPIII inhibition (Fig. 1c-d).

Next, we examined the presence of the three RNAPs within NBS1-positive nucleolar caps. RNAPI was detected in nearly all NBS1-positive caps. However, its recruitment was significantly reduced (by ~35%) in BMH-21-treated cells (Fig. 1e-f), suggesting that RNAPI activity is required for robust recruitment to a subset of nucleolar caps. In contrast, neither THZ1 nor the RNAPIII inhibitor affected RNAPI localization to these caps (Fig. 1e-f).

162 RNAPII recruitment, assessed via phosphorylation of serine 5 on its C-terminal domain (CTD
163 S5P)—a marker of transcriptional initiation by RNAPII—was observed in approximately 21% of
164 NBS1-positive nucleolar caps (Fig. 1g-h). This is consistent with our previous findings suggesting
165 that these rDNA foci may undergo repair via the HR pathway[9] . Notably, RNAPII recruitment was
166 not affected by inhibition of either RNAPI or RNAPIII (Fig. 1g-h). Finally, RNAPIII, detected via
167 its RPC32 subunit, was present in only ~8% of NBS1-positive nucleolar caps, and this fraction
168 remained unchanged across all RNAP inhibitor treatments (Fig. S2a-b).
169 Together, these data indicate that while both RNAPI and RNAPII are actively involved in rDNA
170 repair at NBS1-positive nucleolar caps, only RNAPII inhibition significantly impairs the cap
171 formation.
172

173 **RNAPII activity is required for nucleolar cap formation upon rDNA damage**

174 RNA transcription associated with DNA repair by HR is an essential aspect of accurate DSB repair
175 in the nucleoplasm [12]. Moreover, persistent rDNA breaks become relocated out of the nucleoli,
176 thereby avoiding cis-recombination between rDNA copies to preserve the stability of these
177 vulnerable genomic regions. We hypothesized that rDNA DSB relocation to the nucleolar periphery
178 is also required to allow their engagement with specific DNA repair factors, including an active
179 RNAPII for an accurate, HR-mediated DNA break repair. To test this hypothesis, we first
180 monitored nucleolar cap formation after induction of rDNA DSBs using our U2OS-NBS1-GFP-
181 Cas9 system transfected with gRNA vectors and treated with RNAP inhibitors. In these cells, THZ1
182 treatment efficiently reduced S5P of the RNAPII as revealed by nuclear immunofluorescence
183 intensity upon staining with a RNAPII-S5P antibody (Fig. 2b-c) [35]. Inhibition of RNAPII by THZ1
184 blocked initiation and elongation of nascent RNA transcripts and consequently also reduced DNA
185 end resection as the primary step of the HR-mediated DSB repair (Fig. 2d). The reason why THZ1
186 treatment also partly reduces DNA resection in cells transfected by an empty vector instead of
187 gRNA reflects the fact that RNAPII also plays a role in repair of endogenous DNA damage, as we
188 demonstrated previously [12]. Monitoring formation of NBS1-GFP-containing nucleolar caps after
189 transfection of rDNA-specific gRNAs demonstrated that >25% of cells accumulated these
190 structures in the nucleolar periphery by 6 hours after gRNA transfection (Fig. 2e-f). Treatment with
191 THZ1 for 2 hours before the 6-hour cap formation assessment time-point (Fig. 2a) revealed an
192 almost 3-fold decrease in the percentage of cells with NBS1 positive caps (Fig. 2e-f). We also
193 confirmed that RNAPII inhibition impaired the number of NSB1-GFP-positive caps formed per
194 cell, consistent with the requirement of active RNA transcription for efficient cap formation (Fig.
195 2g). In control experiments, we excluded the possibility that Cas9 levels were affected by RNAPII
196 transcription inhibition during the 2 hours of treatment with THZ1 (Fig. 2h).

197 To corroborate the results obtained using stable Cas9 expression in U2OS, we further assayed
198 rDNA DSB behavior in U2OS cells upon transient gRNA transfection and direct transfer of ectopic
199 recombinant Cas9 protein, thereby avoiding the plasmid integration events and potential off-target
200 effects due to stable Cas9 maintenance in the cells. Nucleolar caps formed more rapidly using this
201 transient expression approach compared with the plasmid-based expression system [6]. Indeed, the
202 cells showed nucleolar cap formation already during the first 3 hours after gRNA/Cas9 transfection
203 (Fig. S3a). THZ1 treatment immediately after transfection reduced nucleolar cap formation at 1
204 hour after transfection and even more robustly, up to 4-fold, after 3 hours of THZ1 exposure (Fig.
205 S3a. This approach excludes any possible negative impact of either Cas9 or NBS1-GFP stable
206 expression during THZ1 treatment (Fig. S3b), which might affect S5P phosphorylation of the
207 RNAPII (Fig. S3c).
208 The decrease of RNA transcription initiation upon THZ1 treatment was accompanied by a defective
209 DNA end resection as the primary step of the HR-mediated DSB repair (Fig. 2d), consistent with
210 the dependence of HR repair on nascent RNA synthesis. Taken together, our data suggest that
211 RNAPII inhibition by THZ1 impairs nucleolar cap formation, probably due to the requirement of
212 nascent RNA for efficient assembly, and hence function, of the HR machinery at the nucleolar
213 periphery.
214

215 **Transcription initiation and elongation promote accurate rDNA DSB repair**

216 While THZ1 is a potent specific inhibitor of CDK7, hence blocking the initiation of nascent RNA
217 transcript, we asked if other RNAPII inhibitors targeting CDK7, CDK9, CDK12 and CDK13 would
218 also impair cap formation upon induction of rDNA breaks (Fig. 2i). First, even a 10-fold lower
219 concentration of THZ1 (0.1 μM), reduced the percentage of cells with nucleolar caps and number
220 of caps per cells upon Cas9-induced rDNA DSBs (Fig. 2j-l). THZ531 is a covalent inhibitor of
221 CDK12/CDK13 when used at low concentrations, 158 and 69 nM, respectively, but it can affect
222 CDK7 and CDK9 at high concentrations (>8.5 μM). THZ531 used at a low concentration (1 μM)
223 had a similar effect to that caused by THZ1 in NBS1-GFP-Cas9 cells after gRNA-vectors
224 transfection to generate rDNA breaks, namely a 2-fold decrease of nucleolar cap formation (Fig.
225 2j-l). This effect suggests that transcription elongation promoted by the CDK12/13 kinase-mediated
226 serine 2 phosphorylation of the RNAPII CTD may also contribute to nucleolar cap formation in
227 cells with rDNA DSBs. However, we noticed that THZ531 at this concentration also decreased S5P
228 of the RNAPII CTD domain, similarly to THZ1 (Fig. 2m), suggesting that mainly initiation and,
229 possibly, elongation steps of RNAPII transcription promote cap accumulation. Then, we
230 investigated other CDK9-targeting drugs that operate through different mechanisms. THAL-SNS-
231 032 is a selective CDK9 PROTAC degrader consisting of a CDK-binding SNS-032 ligand linked

232 to a thalidomide derivative that binds the E3 ubiquitin ligase Cereblon (CRBN)[36]. NPV-2 is a potent
233 and selective ATP-competitive inhibitor of CDK9[37] that inhibits RNAPII at low concentrations.
234 Treatment with either of these inhibitors during 2-3 hours before nucleolar cap assessment upon
235 rDNA DSB induction demonstrated that any RNAPII dysfunction in S5P-CTD caused by CDK9
236 inhibition impairs rDNA repair associated with both a decreasing percentage of cells with NBS1-
237 marked nucleolar caps, and the number of caps per cells (Fig. 2j-l). These data indicate that CDK9
238 inhibition causes a deficiency in rDNA repair *via* impairment of RNA transcription. Finally, we
239 used DRB, a classic inhibitor of transcription elongation by RNAPII, yet with a broader spectrum
240 of targets than the other inhibitors used above. DRB treatment also resulted in a lower percentage
241 of cells with NBS1-foci and NBS1-cap structures relative to control DMSO-treated cells (Fig. 2j-
242 l). To minimize the likelihood of any off-target effect of THZ1, we used another known RNAPII
243 inhibitor, triptolide, that affects RNA transcription initiation by RNAPII degradation via
244 proteasome [12, 38]. We observed similar nucleolar cap formation deficiency after triptolide treatment,
245 demonstrating that the inhibition of transcription initiation by RNAPII indeed compromises
246 nucleolar cap formation (Fig. S3d-e). All the RNAPII inhibitory compounds used in this study
247 consistently showed that nascent RNA transcription by RNAPII is essential for cap formation
248 measured by NBS1 accumulation.
249

250 **RNAPII colocalizes with nucleolar caps upon rDNA DSB formation.**

251 Our recent studies showed that transcription initiation promotes HR factor recruitment at whole
252 genome DNA DSBs in nucleoplasm [12, 23, 26, 39]. To further study the relevance of the RNAPII
253 function for rDNA BSB repair, we next wondered if the transcription complexes are recruited
254 actively to the nucleolar caps. We utilized high-resolution fluorescence imaging of NBS1-GFP-
255 Cas9 U2OS cells to assess the colocalization of additional factors at nucleolar caps. First, cells were
256 co-stained with antibodies to transcription initiation markers such as S5P residue in the CTD
257 domain of the RNAPII. As shown in Fig. 3a the RNAPII-S5P staining is pan-nuclear but reveals
258 accumulation in distinct foci close to the nucleolar periphery. To assess whether the transcription
259 initiation complex is located in the nucleolar caps, we analyzed the dynamic profile of rDNA DSBs
260 marked by NBS1-GFP, along with the transcription initiation marker RNAPII-S5P. We observed
261 RNAPII-S5P recruitment to nucleolar caps, significantly colocalizing with NBS1, suggesting that
262 active nascent transcription in these regions is spatially coordinated with rDNA repair (Fig. 3a).
263 Under these conditions, we also detected a later stage of RNA nascent process using S2P of the
264 CTD domains that drives transcription elongation (RNAPII-S2P). RNAPII-S2P remained localised
265 at the nucleolar caps, although it showed a diffuse colocalization pattern in some of them (Fig. 3b).
266 These results suggest that early transcription steps do occur in the vicinity of the rDNA DSBs at

267 the periphery of the nucleolus, consistent with a functional link between active RNAPII and rDNA
268 repair[12]. Finally, we analysed the profile for other phosphorylations in the CTD of the RNAPII,
269 specifically in Tyrosine 1 (RNAPII-Y1P), which some studies have related to DSB repair [25]. Our
270 colocalization analysis showed that RNAPII-Y1P occupancy in the nucleolar caps was limited to
271 the periphery of the rDNA DSB-containing regions marked by NBS1-GFP (Fig. 3c), suggesting
272 that this modification *per se* is unlikely to be directly required for the rDNA repair, despite it is
273 locally connected with the area of RNA-coupled rDNA repair. Taken together, these results suggest
274 a relationship between nascent RNA transcription by RNAPII and nucleolar caps.
275 As we mentioned previously, RNAPIII has recently been associated with promoting HR of DSBs,
276 similarly to RNAPII[23]. Therefore, we analyzed RPC32, an RNAPIII-specific subunit, in further
277 detail. High resolution images showed that RNAPIII does not colocalize completely with NBS1-
278 GFP in the nucleolar caps, but partial colocalization was detected (Fig. S2c) Notably, a subset of
279 nucleolar caps showed a very robust match between NBS1 and RPC32 proteins while other
280 nucleolar caps lacked RPC32 entirely, even in the same cell (Fig. S2c). These results suggest that
281 RNAPII is highly enriched in nucleolar caps, whereas RNAPIII is only partially present and likely
282 plays a more limited, context-dependent role in this process.
283
284 **RNAPII inhibition impairs recruitment of HR factors to nucleolar caps.**
285 The relocation of rDNA DSBs from the nucleolar interior to anchoring points at the nucleolar
286 periphery is thought to render rDNA breaks accessible to repair factors that are excluded from the
287 nucleoli [18]. To gain mechanistic insight into this process, we examined whether DNA resection
288 following CRISPR-induced rDNA DSBs occurs within nucleolar caps and whether this is
289 influenced by RNAPII inhibition. We assessed CtIP localization at NBS1-positive nucleolar caps
290 to determine whether the observed colocalization pattern depends on ongoing transcription. CtIP
291 was detected in over 60% of repair-associated nucleolar caps (Fig. 4a-b), However, treatment with
292 transcription inhibitors such as THZ1, DRB, and Triptolide reduced CtIP recruitment by more than
293 20% (Fig. 4a–b). To confirm these results, we carried out a Proximity Ligation Assay (PLA) to
294 assess recruitment of CtIP after treatment with the RNAPII inhibitor, THZ1. Ribosomal DSBs
295 induction showed interaction between NBS1 and CtIP partially dependent of RNAPII transcription,
296 as suggested by lowered PLA spots after THZ1 treatment (Fig. 4c). Treatment with the RNAPII
297 inhibitor did not alter the cellular CtIP protein level, thereby excluding the possible overall CtIP
298 deficiency under these conditions (Fig. S4a). To rule out the possibility that THZ1 affects other
299 DSB repair factors such as 53BP1, we analyzed its colocalization with NBS1 under the same
300 conditions and found it to be unaffected by RNAPII inhibition (Fig. S4b-c).
301

302 To further evaluate the impact of rDNA resection upon RNAPII inhibition, we detected the ssDNA
303 stretches formed by rDNA end resection. To do so, we employed immunostaining for native BrdU
304 incorporation, reflecting accessibility of the resected 5' DNA strand, an ssDNA intermediate in the
305 HR repair mechanism [12]. Profile analysis showed colocalization peaks for the NBS1-GFP and BrdU
306 staining, indicating an active DNA resection process inside the analysed nucleolar caps (Fig. 4d).
307 We wanted to investigate whether this decrease is likely due to the requirement for RNAPII activity
308 in the nucleolar caps, in order to repair the rDNA breaks by the HR pathway. To validate the activity
309 of RNAPII within the nucleolar caps, we conducted an analysis of nascent RNA incorporation using
310 EU. This analysis provided evidence that RNA transcription occurs inside the nucleolar caps and is
311 necessary for the formation of these rDNA DSB repair structures, as indicated by the colocalization
312 pick of nascent RNA with DNA repair factors such as NBS1 (Fig. 4e). Altogether, our data indicate
313 that the nascent RNA plays a crucial role in recruiting the HR repair machinery in the rDNA
314 chromatin context.
315

316 **Ribosome biogenesis remains unaffected by rDNA Double-Strand Breaks**

317 We demonstrated that RNAPII inhibition under conditions of rDNA DSB generation by CRISPR
318 technology impaired the rDNA damage repair. We therefore wondered whether the treatment with
319 THZ1 might have negatively affected ribosome biogenesis and whether such potential effect would
320 be enhanced upon generation of rDNA DSBs in our model system. To test so, we performed
321 polysome profile analysis. Our results indicate that neither ribosome biogenesis nor translation were
322 significantly affected by the THZ1 treatment, the induction of rDNA double-strand breaks (DSBs),
323 or the combination of both, within 6 hours after gRNA transfection (Fig. 5a, left). At the 24-hours
324 post rDNA DSB induction, the observed polysome profiles primarily reflected the impact of
325 RNAPII inhibition—namely, mRNA depletion—yet, once again, rDNA DSB induction does not
326 appear to disrupt translational activity (Fig. 5a, right). To further analyze the potential consequences
327 of THZ1 treatment for ribosomal biogenesis at 24 hours post rDNA damage induction, we analysed
328 pre-rRNA processing in U2OS cells by assessing the levels of pre- and mature rRNAs by northern
329 blotting (Fig. 5b). As shown in Fig. 5c-d, inhibition of RNAPII significantly affected pre-rRNA
330 processing. Thus, upon THZ1 treatment for 24 hours, an accumulation of early (e.g. 47S/45S pre-
331 rRNAs) and later (e.g. 30S, 32S, 12S pre-rRNAs) pre-rRNAs was observed (Fig. 5c-d). In contrast,
332 steady-state levels of mature 18S and 28S rRNAs remained unaffected upon the treatment, likely
333 reflecting the stable nature of preexisting ribosomes. The functional significance of these pre-rRNA
334 processing alterations is unclear. However, it could be due to limited levels of specific protein
335 assembly factors and/or their function following RNAPII inhibition. Importantly, formation of the
336 CRISPR-induced rDNA DSBs alone neither impeded pre-rRNA transcription nor enhanced the

observed pre-rRNA processing defects induced by THZ1 treatment, indicating that this type of rDNA damage did not reduce the overall number of actively transcribed rDNA copies, a result that was also consistent with the polysome profile data (Fig. 5a). These results indicated that, *per se*, the rDNA damage induced in our model system does not cause any major defects of ribosome biogenesis and function that could influence the interpretation of our results (see Discussion).

CtIP regulates RNAPII recruitment for rDNA repair

To provide more mechanistic insights into the role of RNAPII in nucleolar caps-associated HR of rDNA breakage, we next investigated whether CtIP may facilitate RNAPII recruitment[9] to the rDNA DSBs in our model. Therefore, we knocked down CtIP to determine whether it is similarly required for rDNA repair—especially considering that both RNAPII and CtIP are mostly present in the nucleoplasm. Indeed, silencing CtIP impaired RNAPII recruitment to nucleolar caps following rDNA DSB induction (Fig. 6a-c). Moreover, BRCA1 accumulation in nucleolar caps was also markedly reduced in CtIP-depleted cells, suggesting that CtIP is essential for the recruitment of the DNA resection machinery at these specific sites (Fig. 6d-e). In contrast, localization of the NHEJ factor 53BP1 within nucleolar caps remained unaffected by CtIP silencing and was observed in the majority of nucleolar caps following rDNA damage (Fig. 6f-g). These findings underscore the emerging role of the CtIP–RNAPII axis in HR-mediated repair of rDNA DSBs within nucleolar caps, while highlighting the distinct and CtIP-independent recruitment of NHEJ factors such as 53BP1.

To investigate whether CtIP contributes to RNAPII-dependent transcription at damaged rDNA sites, we assessed levels of H3K36 trimethylation (H3K36me3), a histone mark classically associated with RNAPII transcription elongation and with the recruitment of DNA repair factors at DSBs [40, 41]. Silencing CtIP led to a pronounced reduction in the H3K36me3 immunostaining signal within nucleolar caps (Fig. 7a-b) and a two-fold decrease in the spatial coordination between RNAPII and H3K36me3 at sites of rDNA repair, as measured by colocalization analysis (Fig. 7c). The CtIP/RNAPII deficiency impaired also BRCA1 recruitment to rDNA breaks (Fig. 7d-e), suggesting that H3K36me3 may serve as a critical chromatin signal that facilitates HR factor recruitment and rDNA relocalization during DSB repair. Importantly, we observed an increase in nucleolar-associated H3K36me3 intensity in response to rDNA DSBs induced by CRISPR-based targeting (Fig. S5), supporting a mechanistic model in which co-transcriptional repair of rDNA breaks is coordinated by RNAPII and DNA resection machinery, and regulated through H3K36me3-dependent chromatin remodelling (Fig. 7f).

RNAPII inhibition provokes rDNA instability and cell death in cancer cells.

372 To assess the biological longer-term consequences of rDNA damage upon RNAPII inhibition, we
373 first examined cell survival by clonogenic assay after rDNA DSB induction and THZ1 treatment.
374 Induction of rDNA DSBs resulted in a robust 3-fold reduction of cell colony counts (Fig. 8a),
375 consistent with previous work [42]. Furthermore, THZ1 treatment alone sensitized the undamaged
376 tumor cells, likely because RNAPII inhibition causes endogenous whole genome DNA damage[12].
377 We observed an increased, albeit not synergistic effect on reducing colony formation when
378 combining the rDNA DSB induction with RNAPII inhibition (Fig. 8a and S6a). Additive effects of
379 targeting components of the same pathway can occur, here when rDNA damage is combined with
380 RNAPII inhibitor THZ1, due to the requirement to repair the endogenous DSBs outside rDNA,
381 thereby achieving a stronger blockade of essential processes and ultimately amplifying cell growth
382 inhibition or cell death. To examine this phenotype further, we performed an MTT assay based on
383 the reduction of the tetrazolium salt MTT to a dark-coloured formazan product by metabolically
384 active cells, to obtain complementary assessment of cell viability. The damage in rDNA alone
385 reduced (2-fold) cell viability (Fig. 8b). Likewise, RNAPII inhibition by THZ1 negatively impacted
386 the cell viability of both rDNA-damaged and undamaged cells, with a tendency for an additive
387 effect when rDNA damage and THZ1 treatment were combined (Fig. 8b). The results were similar
388 but more pronounced after 24 hours of THZ1 treatment (Fig. S6b).
389 It is known that nuclear DNA damage can cause mitochondrial dysfunction, and changes in
390 mitochondrial membrane potential may undermine cell viability though apoptosis [43]. Thus, we
391 analysed mitochondrial membrane potential after THZ1 treatment for 2 hours in rDNA-damaged
392 and undamaged cells, but no significant differences were observed (Fig. S6c-d). There was a
393 modest, non-significant decrease in membrane potential in cells treated with THZ1 for 24 hours
394 (Fig. S6e). As THZ1 impairs nucleolar cap formation, and defective DNA repair usually leads to
395 an increase in genomic instability, we next investigated whether RNAPII inhibition after rDNA
396 DSB induction may impact genome stability. For this purpose, we analysed micronuclei formation
397 frequency, one of the indicators of genome instability due to DNA damage [44]. After rDNA DSB
398 induction, a 2-fold increase of micronuclei formation was observed (Fig. 8c), further enhanced by
399 RNAPII inhibition upon THZ1 treatment (Fig. 8c-d). Notably, rDNA regions were present in the
400 formed micronuclei after rDNA lesion induction and transcription inhibition conditions (Fig. 8d).
401 After 24 hours of THZ1 treatment, the micronuclei formation results were similar (Fig. S6f).
402 Altogether, our results emphasise the importance of rDNA repair under genotoxic nucleolar stress
403 and highlight the important role of RNAPII in the maintenance of nucleolar homeostasis and rDNA
404 stability.
405
406

407 **Discussion**
408
409 Ribosomal DNA represents one of the most transcriptionally active and repetitive genomic regions,
410 inherently prone to instability under replicative or transcriptional stress, a condition frequently
411 amplified in cancer cells due to deregulated ribosome biogenesis and elevated protein synthesis [1–
412 3]. While being transcriptionally dominated by RNAPI, rDNA is also susceptible to DNA DSBs,
413 particularly at the intersection of replication and transcription machinery [6,7]. The rDNA lesions pose
414 a unique challenge due to the repetitive nature of rDNA, requiring specialized repair pathways to
415 prevent catastrophic chromosomal rearrangements [8,14,35].
416 Although RNAPII was not previously thought to function in the nucleolus, it has recently been
417 shown to regulate RNAPI transcription and, under genotoxic stress, driving transcription of the
418 rDNA intergenic spacer to sequester aberrant transcripts for DNA repair [31, 32]. However, whether
419 RNAPII contributes to the regulation of the specialized nucleolar nDDR remains unclear, and in
420 this work, we extend its role by demonstrating its relevance in maintaining genomic stability within
421 this region. Our findings demonstrate an active presence of RNAPII to rDNA regions that are not
422 transcribed by RNAPI, suggesting a functional role beyond passive association. This support
423 previous data about the role of RNAPII in DNA resection on untranscribed regions [12, 26, 27], and not
424 just in active region [21, 45], including rDNA genes. Furthermore, our data aligns with emerging
425 evidence supporting a complementary role for RNAPII within the nucleolus alongside RNAPI [31,
426 32].
427 This process is orchestrated via a transcription-coupled mechanism involving RNAPII recruitment
428 to nucleolar caps, perinucleolar structures that serve as peripheral subdomains for active DNA
429 repair [20, 34, 46]. Pharmacological inhibition of RNAPII by CDK7 (THZ1), CDK9, CDK12/13
430 inhibitors, as well as elongation blockers (DRB, triptolide), significantly impaired nucleolar cap
431 formation and HR factor assembly, highlighting a transcription-dependent switch for pathway
432 engagement. These findings extend earlier work that identified RNAPII as a determinant of repair
433 pathway choice at nucloplasmic DSBs [4,9,20], now applied to the nucleolar context.
434 Mechanistically, we show that transcription initiation, and likely also elongation, are necessary for
435 efficient recruitment of RNAPII to rDNA damage foci, as reflected by Ser5 and Ser2
436 phosphorylation of its C-terminal domain (CTD), respectively. Pharmacological inhibition of these
437 critical regulatory phosphorylations of RNAPII abrogates the early assembly of HR components.
438 The co-localization of NBS1 with markers of transcriptionally active RNAPII confirms that rDNA
439 lesions are transcriptionally licensed for repair, consistent with previous models where nascent
440 RNA guides HR machinery to nucleoplasmic DSBs *via* RNA–protein scaffolds. [9,20,26,27]
441 Furthermore, our high-resolution imaging and biochemical data confirm that CtIP acts as a master
442 regulator in this rDNA repair mechanism. Knock-down of CtIP not only prevented RNAPII

443 recruitment but also reduced H3K36me3 levels at nucleolar caps, a chromatin modification
444 catalyzed by SETD2 and essential for BRCA1 loading and HR progression [33,34,42]. The latter result
445 underscores a previously uncharacterized role for CtIP in controlling transcription-coupled
446 chromatin remodeling in the nucleolus, acting upstream of RNAPII-SETD2 in rDNA repair. These
447 data are consistent with reports positioning CtIP as a cofactor for DNA end resection, acting in
448 concert with the MRN complex and CDK-dependent phosphorylation to license HR [39–41]. Our data
449 also showed that the CtIP-dependent reduction in H3K36me3 levels following rDNA damage has
450 significant implications for rDNA repair pathway choice, highlighting the role of this histone mark
451 in chromatin remodeling specifically at rDNA loci. These results therefore establish a transcription–
452 chromatin modification axis that is both spatially and mechanistically linked to HR engagement at
453 ribosomal chromatin. The increase in H3K36me3 levels upon CRISPR-induced rDNA DSBs
454 further strengthens this model, suggesting that damage-induced modulation of certain chromatin
455 states facilitate rDNA repair.
456 Interestingly, the mechanism elucidated in our present study appears to be exclusive to RNAPII, as
457 inhibition of either RNAPI and or RNAPIII did not impact nucleolar cap formation. This is in line
458 with recent data positioning RNAPIII as a context-dependent factor in DSB repair [4], and with the
459 known role of RNAPII in producing nascent transcripts that scaffold HR complexes at DNA breaks
460 [9,20,26]. Although RNAPIII components were occasionally detected in nucleolar caps, their
461 inconsistent localization suggests a supportive, rather than central, role in rDNA repair—potentially
462 influenced by local chromatin environments or transcriptional states [4,18].
463 Our data also support a model in which persistent rDNA DSBs that are not repaired by NHEJ inside
464 the nucleoli become selectively relocated to nucleolar caps for repair, reinforcing prior reports that
465 nucleolar stress triggers spatial segregation of damaged rDNA to the nucleolar periphery[47-49 15–
466 17,21]. Inhibiting RNAPII function not only impairs such rDNA relocation but also reduces the
467 recruitment of early repair factors such as CtIP. This is consistent with prior work highlighting the
468 interdependence of transcription and DNA end resection in HR activation.[9,20,40,41]
469 Importantly, we show that RNAPII inhibition compromises genome stability and cell viability,
470 particularly in the context of rDNA damage. Increased micronuclei formation following combined
471 RNAPII inhibition and rDNA DSB induction highlights the genomic consequences of defective
472 rDNA repair[44] .Such micronuclei frequently contained rDNA, indicating that unresolved breaks in
473 ribosomal chromatin contribute to chromosomal fragmentation and mitotic errors—phenomena
474 tightly associated with tumorigenesis [30,32,36].
475 Despite the central role of rDNA in ribosome biogenesis, we show that rDNA instability does not
476 necessarily translate into immediate disruption of ribosomal function. Indeed, our data reveal that
477 CRISPR-induced rDNA DSBs do not perturb rRNA transcription, processing, or polysome

478 formation within short-term experiments. Only when RNAPII activity is inhibited we observed
479 defects in rRNA maturation and translation, consistent with the broader role of RNAPII in
480 transcriptional regulation of ribosome assembly factors and non-coding RNAs, including snoRNAs
481 [43,49]. These observations indicate that the genome maintenance function of RNAPII in rDNA repair
482 is separable from its canonical transcriptional roles—at least over acute timescales.
483 Together, our findings define a previously unrecognized co-transcriptional mechanism that
484 safeguards ribosomal genome integrity. We propose a model in which CtIP enables RNAPII access
485 to damaged rDNA regions, promoting H3K36me3 deposition and BRCA1 loading within nucleolar
486 caps. This orchestrated response coordinates spatial repositioning of rDNA breaks with
487 transcriptional and chromatin-based repair signals. The broader implication of our present data is
488 that transcription-coupled HR-mediated DNA DSB repair extends beyond the coding sequences in
489 gene bodies and includes also repetitive, non-coding genomic compartments such as the nucleolus,
490 thereby redefining our understanding of the genome surveillance landscape.
491
492
493
494 **Materials and Methods**
495
496
497 **Cell culture**
498 U2O-Cas9-NBS1-GFP cells [34] were cultured in Dulbecco's Modified Eagle Medium (DMEM) with
499 high glucose plus GlutaMax supplemented with 10% fetal bovine serum (FBS; Biowest), 100 U/ml
500 penicillin and 100 µg/ml streptomycin (Biowest) at 37 °C in 5% CO_2. U2O-Cas9-NBS1-GFP stably
501 transfected cells were maintained by adding 1 µg/ml puromycin and 0.5 mg/ml neomycin G418 to
502 the medium. siRNAs against CtIP (GCUAAAACAGGAACGAAUC) and a control non-targeting
503 siRNA sequence (Sigma Aldrich) were transfected with the RNAiMax lipofectamine reagent mix
504 (Life Technologies), according to the manufacturer's instructions. Cells were cultured in the
505 presence of different inhibitors (Table 1) using concentrations mentioned in each figure.
506
507 **Plasmids and transfections**
508 For rDNA DSB induction by CRISPR/Cas9, four guide RNAs (gRNA) plasmids were used [46].
509 Three of them were pMA plasmids expressing sequences targeting rDNA present on all five
510 acrocentric short arms (Table 2) and the other was a control plasmid expressing the gRNA scaffold
511 but no target sequence. Plasmids carry out ampicillin resistant marker.
512 Transient transfection of U2OS-Cas9-NBS1-GFP cells was carried out using Lipofectamine LTX
513 with plus reagent (Invitrogen) following manufacturer's instructions. Briefly, cells were seeded in
514 different plate formats, accordingly to the requirements of each specific experiment, to be 70-90%

515 confluent at transfection. Then, the three gRNA plasmids pooled in a ratio 1:1:1 and PLUS reagent
516 were diluted in Opti-MEM and mixed with Lipofectamine LTX Reagent blended into Opti-MEM,
517 in a 1:1 ratio. Solution was incubated 5 min at room temperature and finally was added dropwise
518 to the plate with gentle rocking. Cells were then collected 0-6 hours after transfection unless
519 otherwise indicated.
520

521 **Inmunofluorescence**

522 Cells were grown on sterile coverslips, transfected with gRNAs as previously described and treated
523 or not with inhibitors as indicated in each figure. Cells were fixed with 4% paraformaldehyde (w/v)
524 in PBS for 10 min, washed twice with PBS and then permeabilised with 0.2% Triton X-100 in PBS
525 for 5 min. Following two washes with PBS, cells were blocked for at least 1 hour with 5% FBS
526 diluted in PBS, incubated with adequate primary antibodies (Table 3) diluted in 5% FBS in PBS
527 for 2 hours at room temperature, washed again with PBS and then, incubated with the appropriate
528 secondary antibodies (Table 3) and 4′-6-diamidino-2-phenylindole (DAPI, 10 ng/ml) in blocking
529 buffer for 1 hour at room temperature in the dark. Coverslips were mounted with Fluoromount-G
530 mounting medium (Invitrogen), and images were acquired using a LEICA microscope. Image
531 analysis was performed using ImageJ software by quantifying the number of nucleolar caps,
532 nucleolar mean intensity, and fluorescence intensity profiles. Intensity profiles were obtained by
533 drawing a line ROI across the image and using the 'Plot Profile' tool to generate a graph of intensity
534 values along the line. Experiments were repeated at least three times independently.
535

536 **High-content image acquisition**

537 Quantitative image-based cytometry (QIBC) was performed as previously described [12]. Briefly, the
538 images were acquired in an automatic and unbiased way by scanR acquisition software 3.0 (Leica)
539 and analysed by scanR image analysis software 3.0. The results were exported as txt files. The txt
540 data set was further processed with spotfire and PRISM 8 software (Graphpad Software Inc) for
541 further analysis. Statistical significance was determined with Ordinary one-way and two-way
542 ANOVA tests using multiple comparisons using PRISM 8 software (Graphpad Software Inc).
543

544 **Metabolic labeling of nascent RNA by EU**

545 Nascent RNA was visualized using metabolic labeling using Invitrogen™ Click-iT™ RNA Alexa
546 Fluor™ 594 imaging kit, with modifications. Briefly, U2OS-Cas9-NBS1-GFP cells were seeded
547 onto coverslips, transfected with gRNAs as previously described, treated 2 hours with 1 μM of
548 THZ1 inhibitor 4 hours after transfection and pulsed for 30 min with EU at a final concentration of
549 1 mM. Following treatments, cells were fixed with 4% paraformaldehyde (PFA) for 10 min,

550 permeabilised with 0.5% Triton X-100 and washed 3 times with Tris buffered saline (TBS) (50 mM
551 Tris-HCl pH 8.0, 150 mM NaCl). Then, samples were incubated 30 min with fresh prepared Click-
552 iT reaction cocktail, containing 5 µM Alexa Fluor 594 azide, 2 mM CuSO4 and 100 mM sodium
553 ascorbate. After removal of the reaction cocktail, cells were washed three times with TBS and
554 stained with DAPI. Finally, coverslips were mounted onto glass slides using Fluoromount-G
555 (Invitrogen) and cells were imaged by fluorescence microscopy. Image analysis was performed by
556 measuring the intensity profile using the ImageJ software drawing a line ROI over the image and
557 using the "Plot Profile" tool to generate a graph of intensity values along that line.
558

559 **Immunoblotting**

560 Whole-cell extracts were prepared in Laemmli buffer 2X (4% SDS, 20 % glycerol, 125 mM
561 Tris−HCl, pH 6.8, 0.02% bromophenol blue, 200 mM DTT) by boiling at 100 °C for 10 min and
562 sonicated in a Bioruptor for 2 cycles of 30 sec ON/30 sec OFF at high intensity. Proteins were
563 resolved by SDS-PAGE and transferred to nitrocellulose membranes (AmershamTM Protran® 0.45
564 µm, GE Healthcare). Membranes were blocked for 1 hour with 5% BSA in TTBS (15 mM Tris-
565 HCl, pH 7.5, 200 mM NaCl, 0.1% (v/v) Tween-20), followed by incubation with the appropriate
566 primary antibodies overnight at 4°C (Table 3). After being washed with TTBS, membranes were
567 incubated with HRP-conjugated secondary antibodies (Table 3) for 1 hour at room temperature.
568 Chemiluminescence was performed using Clarity Western ECL Substrate (Bio-Rad), and results
569 were acquired using the ChemiDoc Touch Imaging System (Bio-Rad) and visualised with Image
570 Lab software 5.1 (Bio-Rad).
571

572 **Micronuclei assay**

573 Cells were seeded onto coverslips, transfected with gRNAs as previously described and treated 2
574 hours with 1 µM of THZ1 inhibitor 4 hours after transfection. Following treatment, the medium
575 was replaced by fresh one and cytochalasin B (Sigma-Aldrich) was added at 4 µg/ml. 20 hours
576 post-treatment, cells were fixed in PBS-4% paraformaldehyde 10 min, permeabilised in PBS-0.2%
577 Triton X-100 5 min, blocked 30 min in blocking buffer (PBS-5% FBS) and incubated 1-2 hours
578 with nucleolin primary antibody (Table 3) in blocking buffer. Cells were then washed two times
579 with PBS and incubated for 45 min with the corresponding secondary antibody (Table 3) diluted in
580 blocking buffer plus DAPI (Sigma-Aldrich) in darkness. Finally, coverslips were washed twice
581 with PBS, dried and mounted onto glass slides using Fluoromount-G (Invitrogen). Micronuclei
582 containing or not nucleolin were counted only from binucleated cells.
583
584

585

586 **Clonogenic survival assay**

587 For clonogenic survival assays, cells were transfected with gRNA as previously described for rDNA
588 DSBs induction and 4 hours post-transfection cells were treated with different concentration (0.1
589 μM, 0.5 μM, 1μM) of THZ1 or vehicle (DMSO) as control for 2 hours. Then, cells were counted
590 and re-seeded in 6-well plates at two different concentrations, 1000 and 500 cells per well, in
591 triplicates. Cells were then grown at 37º C for 7-8 days to allow colonies formation. Afterwards,
592 plates were washed in PBS and fixed and visualised by staining with 1% methylene blue diluted in
593 20% ethanol, followed by washes with water to remove the excess of staining. Plates were left to
594 dry overnight and the number of colonies per well was scored for each condition and normalised to
595 the untreated condition.

596

597 **MTT assay**

598 MTT [3-(4,5-dimethylthiazol-2-yl)-2,5-diphenyltetrazolium bromide] assay (Roche) was
599 performed following manufacturer's indications. After transfection with gRNA and incubation with
600 different concentration (0.1 μM, 0.5 μM, 1 μM) of THZ1 or DMSO for 2 hours as previously
601 described, cells were seeded at a density of 2×10^3 cells/well in 100 μl of medium on a 96-well plate
602 in triplicates. After 5 days growing, 10 μl of MTT (5 mg/ml) was added to each well, and plates
603 were incubated at 37°C for 4 hours. Then, 100 μl of 10% SDS was added, and cells were incubated
604 overnight at 37°C to dissolve the insoluble purple formazan products. A_{570} was measured using a
605 microplate reader with a reference wavelength of 690 nm.

606

607 **PLA assay**

608 Proximity ligation assay (PLA) was performed using the Duolink In Situ Red Starter Kit
609 Mouse/Rabbit (Sigma-Aldrich) according to the manufacturer's instructions. First, U2OS-Cas9-
610 NBS1-GFP cells were processed like immunofluorescence, blocked with blocking solution from
611 the Duolink PLA Kit for 30 min at 37 °C and staining with specific primary antibodies (Table 3)
612 overnight at 4° C. After that, cells were incubated with MINUS and PLUS secondary PLA probes
613 for 1 h at 37 °C, and the detection of these probes was carried out using the ScanR microscope
614 (Olympus). The number of PLA signals per nucleus was scored in at least 100 cells per sample.

615

616

617 **References**

618 1. Zisi, A., Bartek, J. & Lindstrom, M.S. Targeting Ribosome Biogenesis in Cancer: Lessons
619 Learned and Way Forward. *Cancers (Basel)* **14** (2022).
620 2. Derenzini, M. *et al.* Nucleolar function and size in cancer cells. *Am J Pathol* **152**, 1291-
621 1297 (1998).
622 3. Weeks, S.E., Metge, B.J. & Samant, R.S. The nucleolus: a central response hub for the
623 stressors that drive cancer progression. *Cell Mol Life Sci* **76**, 4511-4524 (2019).
624 4. Hilton, J. *et al.* Results of the phase I CCTG IND.231 trial of CX-5461 in patients with
625 advanced solid tumors enriched for DNA-repair deficiencies. *Nat Commun* **13**, 3607 (2022).
626 5. Lin, Y.L. & Pasero, P. Interference between DNA replication and transcription as a cause
627 of genomic instability. *Curr Genomics* **13**, 65-73 (2012).
628 6. Warner, J.R. The economics of ribosome biosynthesis in yeast. *Trends Biochem Sci* **24**, 437-
629 440 (1999).
630 7. Moss, T. & Stefanovsky, V.Y. At the center of eukaryotic life. *Cell* **109**, 545-548 (2002).
631 8. Bowry, A., Kelly, R.D.W. & Petermann, E. Hypertranscription and replication stress in
632 cancer. *Trends Cancer* **7**, 863-877 (2021).
633 9. Kotsantis, P. *et al.* Increased global transcription activity as a mechanism of replication
634 stress in cancer. *Nat Commun* **7**, 13087 (2016).
635 10. Curti, L. *et al.* CDK12 controls transcription at damaged genes and prevents MYC-induced
636 transcription-replication conflicts. *Nat Commun* **15**, 7100 (2024).
637 11. Korsholm, L.M. *et al.* Recent advances in the nucleolar responses to DNA double-strand
638 breaks. *Nucleic Acids Res* **48**, 9449-9461 (2020).
639 12. Gomez-Cabello, D., Pappas, G., Aguilar-Morante, D., Dinant, C. & Bartek, J. CtIP-
640 dependent nascent RNA expression flanking DNA breaks guides the choice of DNA repair
641 pathway. *Nat Commun* **13**, 5303 (2022).
642 13. Gomez-Cabello, D., Jimeno, S., Fernandez-Avila, M.J. & Huertas, P. New tools to study
643 DNA double-strand break repair pathway choice. *PLoS One* **8**, e77206 (2013).
644 14. Jackson, S.P. & Bartek, J. The DNA-damage response in human biology and disease.
645 *Nature* **461**, 1071-1078 (2009).
646 15. Heyer, W.D., Ehmsen, K.T. & Liu, J. Regulation of homologous recombination in
647 eukaryotes. *Annu Rev Genet* **44**, 113-139 (2010).
648 16. Lopez-Saavedra, A. *et al.* A genome-wide screening uncovers the role of CCAR2 as an
649 antagonist of DNA end resection. *Nat Commun* **7**, 12364 (2016).
650 17. Larsen, D.H. & Stucki, M. Nucleolar responses to DNA double-strand breaks. *Nucleic Acids*
651 *Res* **44**, 538-544 (2016).
652 18. van Sluis, M. & McStay, B. A localized nucleolar DNA damage response facilitates
653 recruitment of the homology-directed repair machinery independent of cell cycle stage.
654 *Genes Dev* **29**, 1151-1163 (2015).
655 19. Kruhlak, M. *et al.* The ATM repair pathway inhibits RNA polymerase I transcription in
656 response to chromosome breaks. *Nature* **447**, 730-734 (2007).
657 20. Larsen, D.H. *et al.* The NBS1-Treacle complex controls ribosomal RNA transcription in
658 response to DNA damage. *Nat Cell Biol* **16**, 792-803 (2014).
659 21. Lesage, E., Clouaire, T. & Legube, G. Repair of DNA double-strand breaks in RNAPI- and
660 RNAPII-transcribed loci. *DNA Repair (Amst)* **104**, 103139 (2021).
661 22. Gal, Z. *et al.* Hyper-recombination in ribosomal DNA is driven by long-range resection-
662 independent RAD51 accumulation. *Nat Commun* **15**, 7797 (2024).
663 23. Liu, S. *et al.* RNA polymerase III is required for the repair of DNA double-strand breaks by
664 homologous recombination. *Cell* **184**, 1314-1329 e1310 (2021).
665 24. Domingo-Prim, J. *et al.* EXOSC10 is required for RPA assembly and controlled DNA end
666 resection at DNA double-strand breaks. *Nat Commun* **10**, 2135 (2019).

667 25. Burger, K., Schlackow, M. & Gullerova, M. Tyrosine kinase c-Abl couples RNA
668 polymerase II transcription to DNA double-strand breaks. *Nucleic Acids Res* **47**, 3467-3484
669 (2019).
670 26. Vitor, A.C. *et al.* Single-molecule imaging of transcription at damaged chromatin. *Sci Adv*
671 **5**, eaau1249 (2019).
672 27. Pappas, G. *et al.* MDC1 maintains active elongation complexes of RNA polymerase II. *Cell*
673 *Rep* **42**, 111979 (2023).
674 28. Cohen, S. *et al.* Senataxin resolves RNA:DNA hybrids forming at DNA double-strand
675 breaks to prevent translocations. *Nat Commun* **9**, 533 (2018).
676 29. Ouyang, J. *et al.* RNA transcripts stimulate homologous recombination by forming DR-
677 loops. *Nature* **594**, 283-288 (2021).
678 30. Bonath, F., Domingo-Prim, J., Tarbier, M., Friedlander, M.R. & Visa, N. Next-generation
679 sequencing reveals two populations of damage-induced small RNAs at endogenous DNA
680 double-strand breaks. *Nucleic Acids Res* **46**, 11869-11882 (2018).
681 31. Abraham, K.J. *et al.* Nucleolar RNA polymerase II drives ribosome biogenesis. *Nature* **585**,
682 298-302 (2020).
683 32. Khosraviani, N. *et al.* Nucleolar Pol II interactome reveals TBPL1, PAF1, and Pol I at
684 intergenic rDNA drive rRNA biogenesis. *Nat Commun* **15**, 9603 (2024).
685 33. Trifault, B. *et al.* Nucleolar detention of NONO shields DNA double-strand breaks from
686 aberrant transcripts. *Nucleic Acids Res* **52**, 3050-3068 (2024).
687 34. Korsholm, L.M. *et al.* Double-strand breaks in ribosomal RNA genes activate a distinct
688 signaling and chromatin response to facilitate nucleolar restructuring and repair. *Nucleic*
689 *Acids Res* **47**, 8019-8035 (2019).
690 35. Nilson, K.A. *et al.* THZ1 Reveals Roles for Cdk7 in Co-transcriptional Capping and
691 Pausing. *Mol Cell* **59**, 576-587 (2015).
692 36. Olson, C.M. *et al.* Pharmacological perturbation of CDK9 using selective CDK9 inhibition
693 or degradation. *Nat Chem Biol* **14**, 163-170 (2018).
694 37. Aoi, Y. *et al.* SPT5 stabilization of promoter-proximal RNA polymerase II. *Mol Cell* **81**,
695 4413-4424 e4415 (2021).
696 38. Wang, Y., Lu, J.J., He, L. & Yu, Q. Triptolide (TPL) inhibits global transcription by
697 inducing proteasome-dependent degradation of RNA polymerase II (Pol II). *PLoS One* **6**,
698 e23993 (2011).
699 39. Meisenberg, C. *et al.* Repression of Transcription at DNA Breaks Requires Cohesin
700 throughout Interphase and Prevents Genome Instability. *Mol Cell* **73**, 212-223 e217 (2019).
701 40. Carvalho, S. *et al.* SETD2 is required for DNA double-strand break repair and activation of
702 the p53-mediated checkpoint. *Elife* **3**, e02482 (2014).
703 41. Markert, J.W., Soffers, J.H. & Farnung, L. Structural basis of H3K36 trimethylation by
704 SETD2 during chromatin transcription. *Science* **387**, 528-533 (2025).
705 42. Warmerdam, D.O., van den Berg, J. & Medema, R.H. Breaks in the 45S rDNA Lead to
706 Recombination-Mediated Loss of Repeats. *Cell Rep* **14**, 2519-2527 (2016).
707 43. Wang, K. *et al.* Blockage of Autophagic Flux and Induction of Mitochondria Fragmentation
708 by Paroxetine Hydrochloride in Lung Cancer Cells Promotes Apoptosis via the ROS-
709 MAPK Pathway. *Front Cell Dev Biol* **7**, 397 (2019).
710 44. Hatch, E.M., Fischer, A.H., Deerinck, T.J. & Hetzer, M.W. Catastrophic nuclear envelope
711 collapse in cancer cell micronuclei. *Cell* **154**, 47-60 (2013).
712 45. Saur, F. *et al.* Transcriptional repression facilitates RNA:DNA hybrid accumulation at DNA
713 double-strand breaks. *Nat Cell Biol* (2025).
714 46. van Sluis, M. & McStay, B. Nucleolar reorganization in response to rDNA damage. *Curr*
715 *Opin Cell Biol* **46**, 81-86 (2017).
716 47. Imrichova, T. *et al.* Dynamic PML protein nucleolar associations with persistent DNA
717 damage lesions in response to nucleolar stress and senescence-inducing stimuli. *Aging*
718 *(Albany NY)* **11**, 7206-7235 (2019).

48. Hornofova, T. *et al.* Phospho-SIM and exon8b of PML protein regulate formation of doxorubicin-induced rDNA-PML compartment. *DNA Repair (Amst)* **114**, 103319 (2022).
49. Urbancokova, A. *et al.* Topological stress triggers persistent DNA lesions in ribosomal DNA with ensuing formation of PML-nucleolar compartment. *Elife* **12** (2024).

Acknowledgments

Thanks to Fernando Gómez Herreros´s lab for helpful discussions. Thanks to Diana Aguilar-Morante and Oliver Quevedo for technical advice and discussions.

Funding:

AECC-Investigator Grant (INVES20017GOME)
University of Seville-Plan Propio-Grant: 2021/00001263 (PV, GS)
MSCA-IF-2017 (795930)
PID2022-137280OB-I00
CNS2023-143939
R+D+i PID2022-136564NB-I00 (MCIN/AEI/10.13039/501100011033 and ERDF/UE "A way of making Europe")
Andalusian Regional Government (P20_00581, BIO-271)
University of Seville (US-1380394, US/JUNTA/FEDER,UE).
Novo Nordisk Foundation (NNF20OC0060590)
Danish Council for Independent Research (DFF-7016-00313)
Swedish Research Council (VR-MH 2014-46602-117891-30)
Danish National Research Foundation (project CARD, DNRF 125)
Danish Cancer Society (R204-A12617-B153)

Author contributions:

Conceptualisation: DGC, JB
Methodology: CCR, BSQ, OQ, LC, DGC
Investigation: JCD, JB, DGC
Supervision: DGC
Writing—original draft: DGC
Writing—review & editing: CCR, DHL, JCD, JB, DGC

Competing interests: The authors declare no competing interests.

Data and materials availability: All data, code, and materials used in the analyses must be available in some form to any researcher for purposes of reproducing or extending the analyses.

774 **Table 1. RNAPs inhibitors**

Drug	Reference	Commercial	Use Concentration	Time of treatment
THZ1	532372	CalbioChem	1 μM	2 hours
THZ531	HY-103618-	MedChemExpress	1 μM	2 hours
NPV2	1702809-17-3	R&D systems	250 nM	3 hours
THAL-SNS032	6532/5	R&D systems	250 nM	3 hours
DRB	D1916	Sigma	100 μM	2 hours
Triptolide	T3652	Sigma	10 μM	30 min
BMH-21				
ML-60218				

775 **Table 2. sgRNA sequences.**

CRISPR vector	Sequence (5´-3´)
rDNA gRNA1	GCGAGAACAGCAGGCCCGC
rDNA gRNA2	GCCTTCTCTAGCGATCTGAG
rDNA gRNA3	GATTTCCAGGGACGGCGCCT

776
777
778
779
780
781
782
783
784
785
786
787
788
789
790
791
792
793
794
795
796
797
798
799
800
801
802

803 **Table 3: Antibodies.**

Antibody	Species	Reference / Suppliers	Application
Nucleolin	Rabbit	Abcam; ab70493	IF (1:1000)
Cas9	Mouse	Abcam; ab191468	WB (1:1000)
β-importin	Mouse	Abcam; ab2811	WB (1:5000)
RNAPII	Mouse	Abcam; ab817	IF (1:1000)
RNAPII S5P	Rabbit	Abcam; ab5131	IF (1:2000)
RNAPII S2P	Rabbit	Abcam; ab5095	IF (1:2000)
RNAPII pY1	Mouse	Active Motif; 61383	IF (1:1000)
BrdU	Rat	Bio-rad AbD Serotec; OBT0030	IF (1:500)
RNAPIII	Mouse	Santa Cruz; SC-48365	IF (1:500)
CtIP	Mouse	Active Motif; 61141	IF (1:250)/WB (1:500)
53BP1	Rabbit	Novus, NB100-904	IF (1:500)
BRCA1	Mouse	Santa cruz; sc-6954	IF 1:100
H3K36me3	Rabbit	Abcam ab9050	IF 1:500
HRP-conjugated goat anti-mouse IgG (H+L)	Goat	Jackson, 111-035-146	WB (1:5000)
Alexa Fluor 647 anti-rabbit	Goat	Invitrogen, A21245	IF (1:1000)
Alexa Fluor 546 anti-rabbit	Goat	Invitrogen, A11010	IF (1:1000)
Alexa Fluor 546 anti-mouse	Goat	Invitrogen, A11003	IF (1:1000)

804

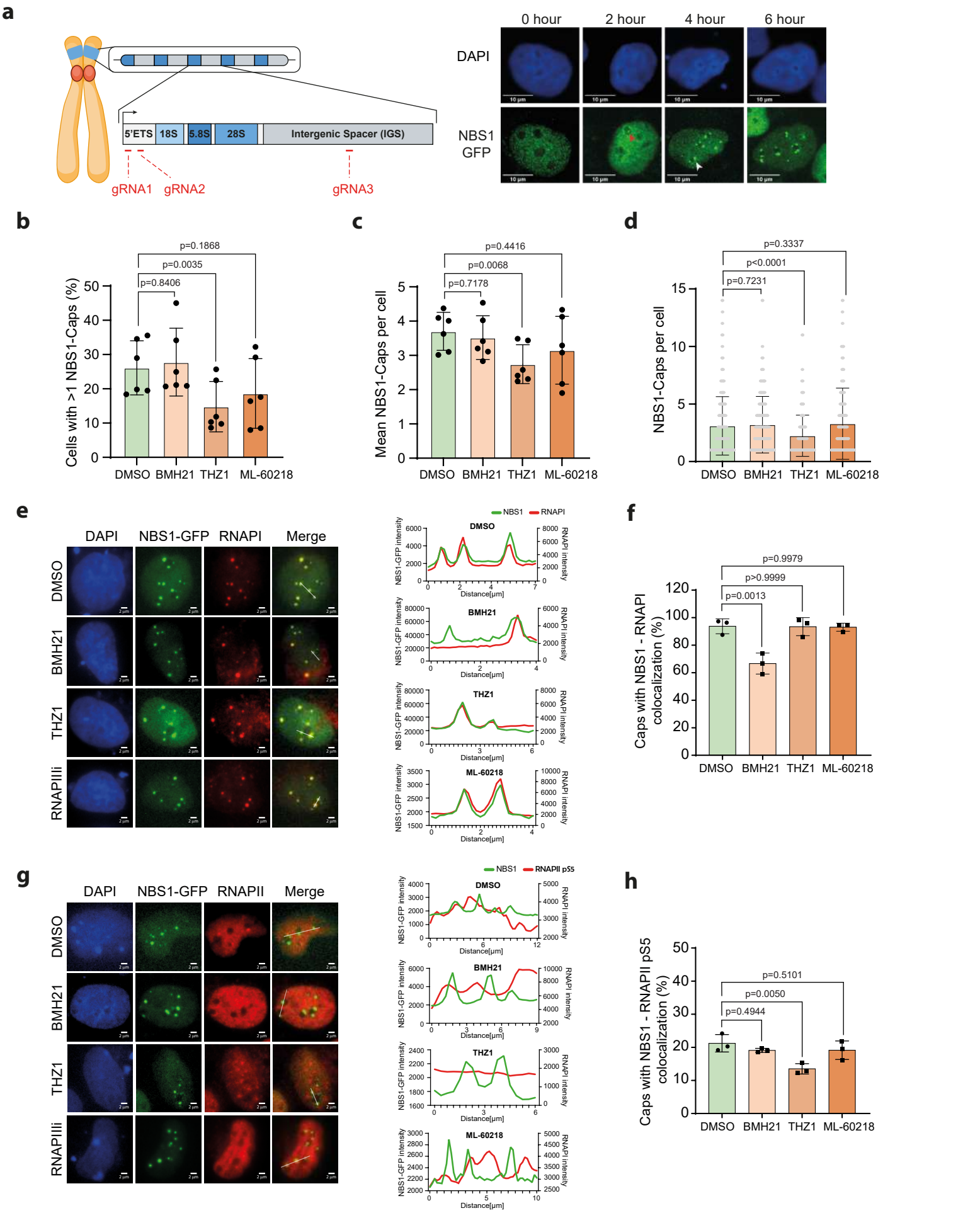

Fig. 1. Checa-Rodríguez, et al.

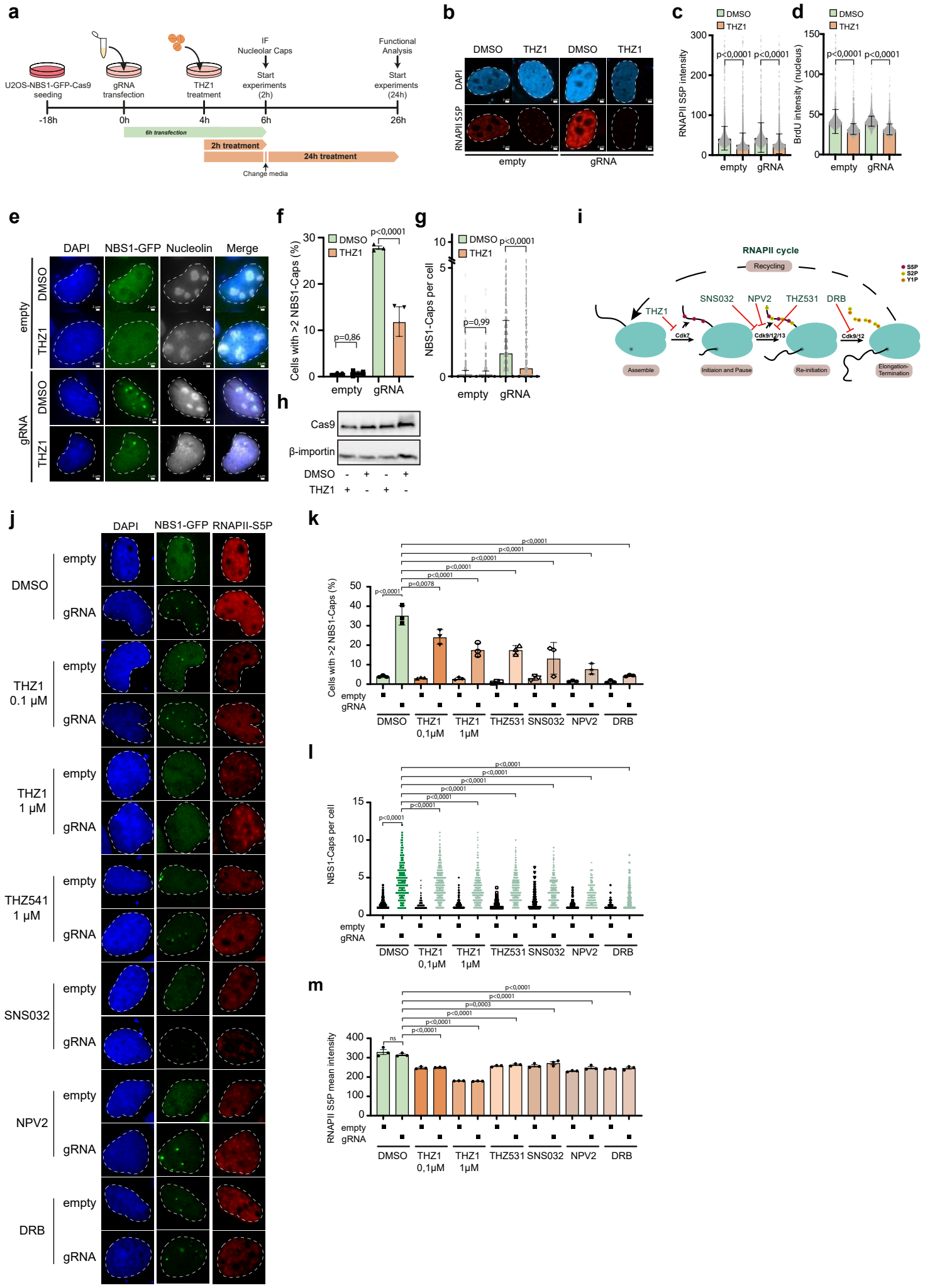

Fig. 2. Checa-Rodríguez, et al.

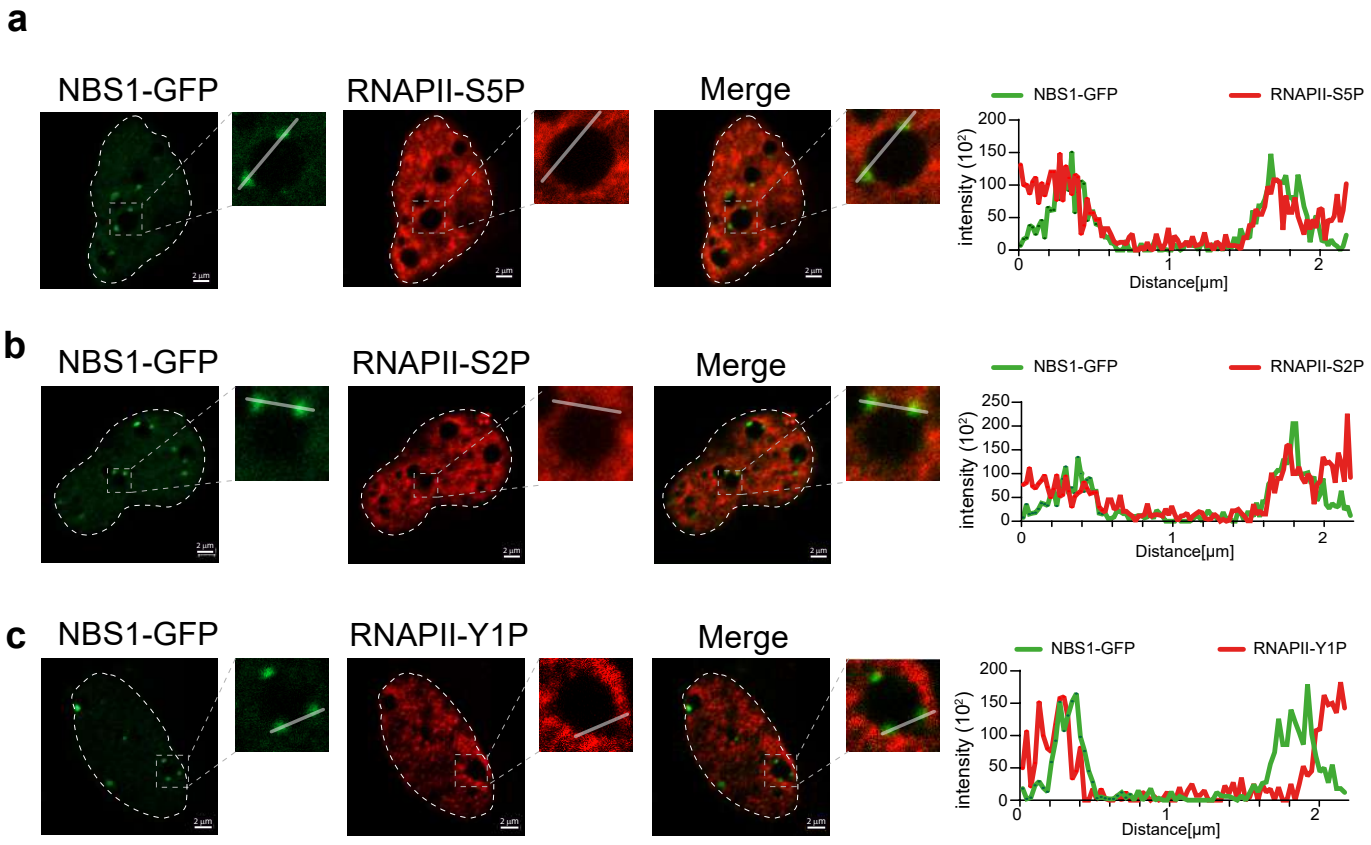

Fig. 3. Checa-Rodríguez, et al.

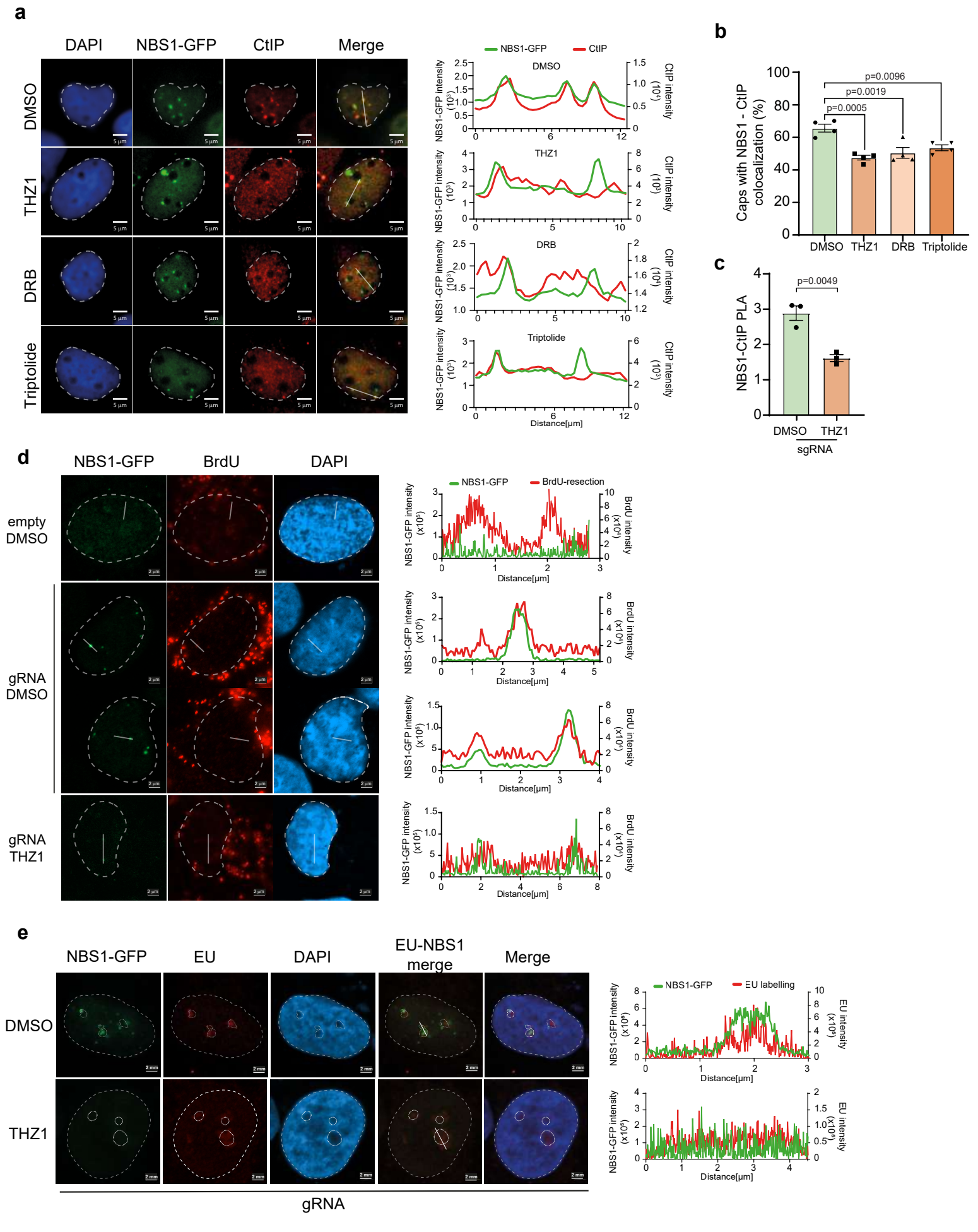

Fig. 4. Checa-Rodríguez, et al.

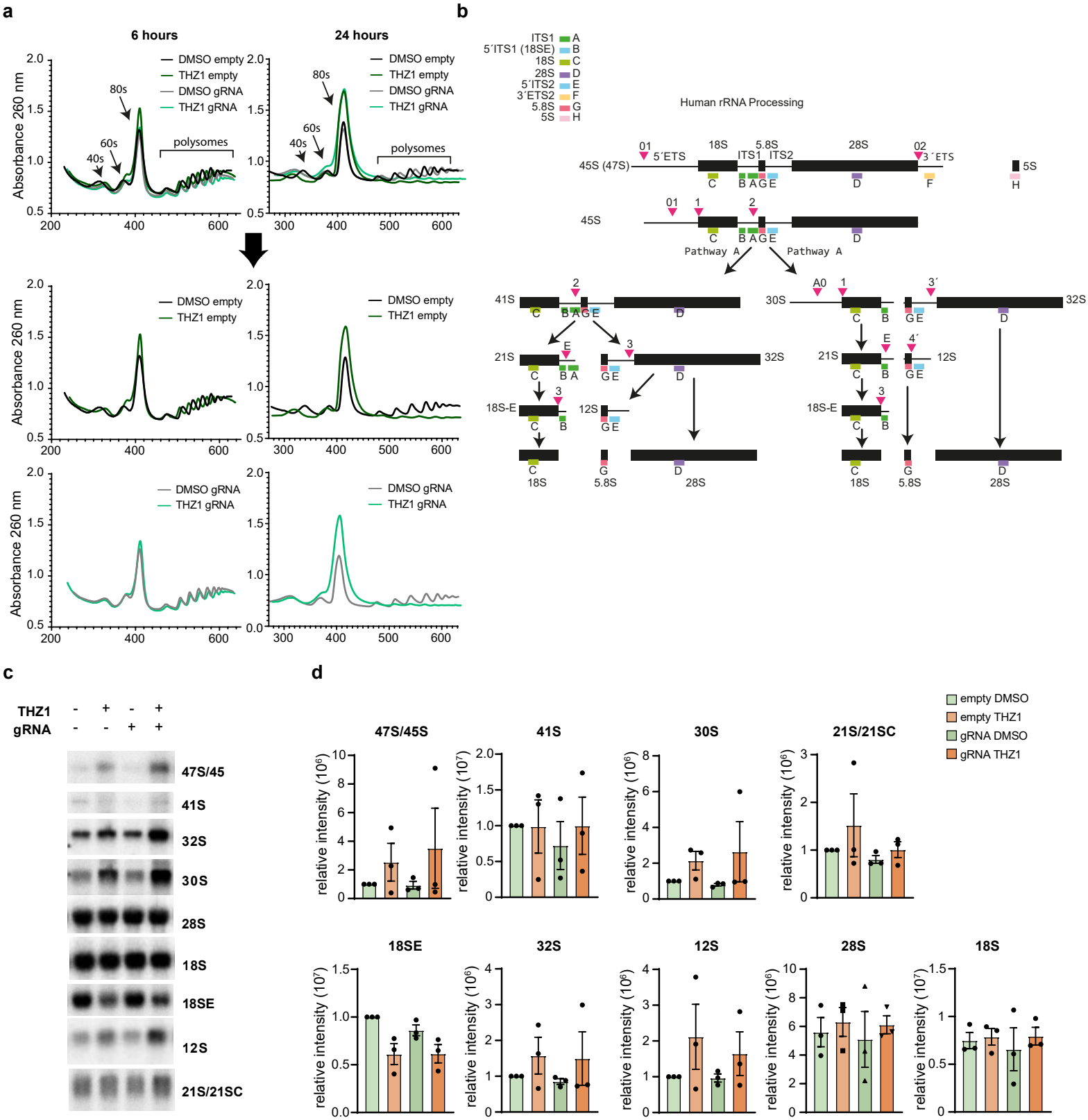

Fig. 5. Checa-Rodríguez, et al.

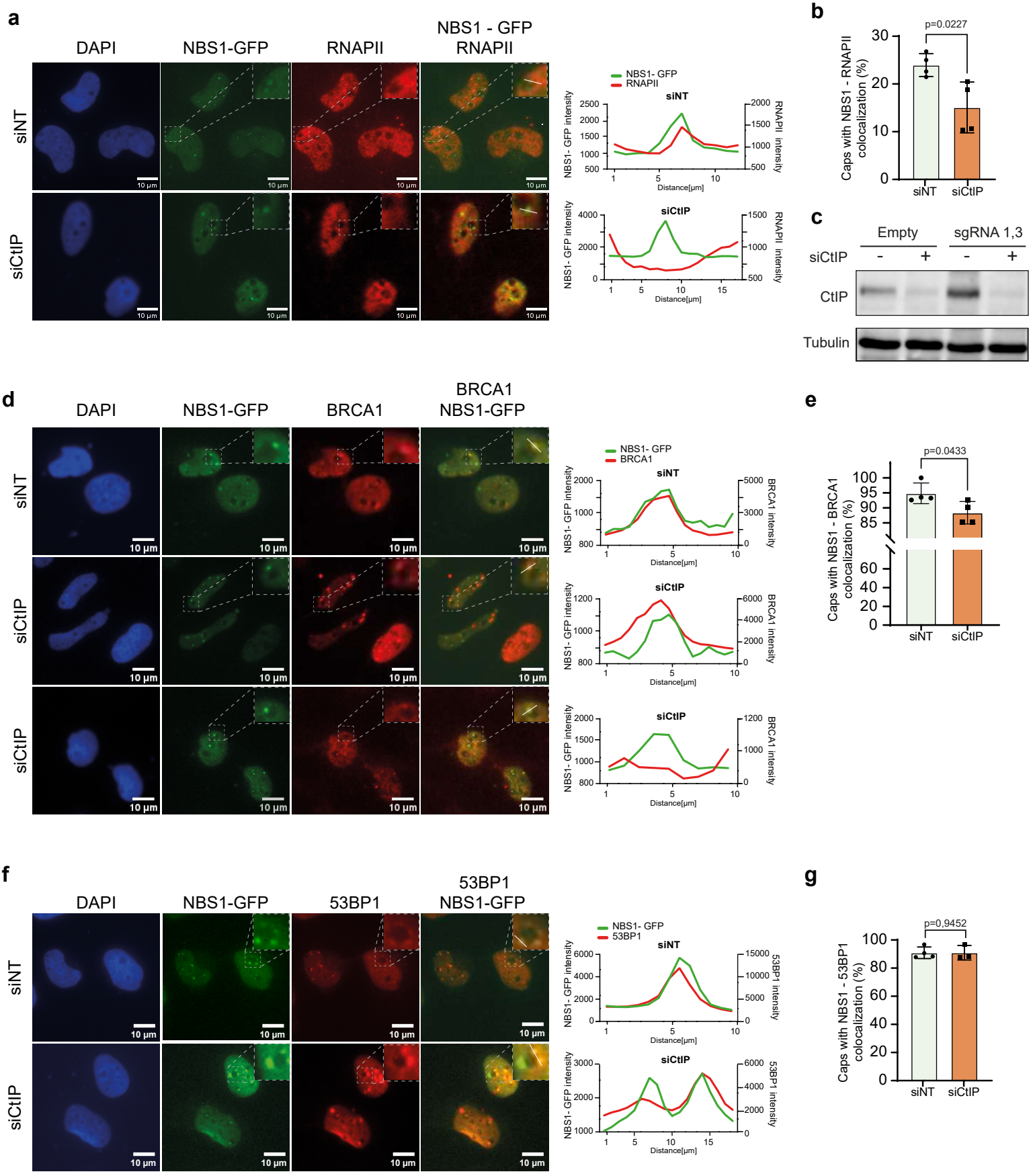

Fig. 6. Checa-Rodríguez, et al.

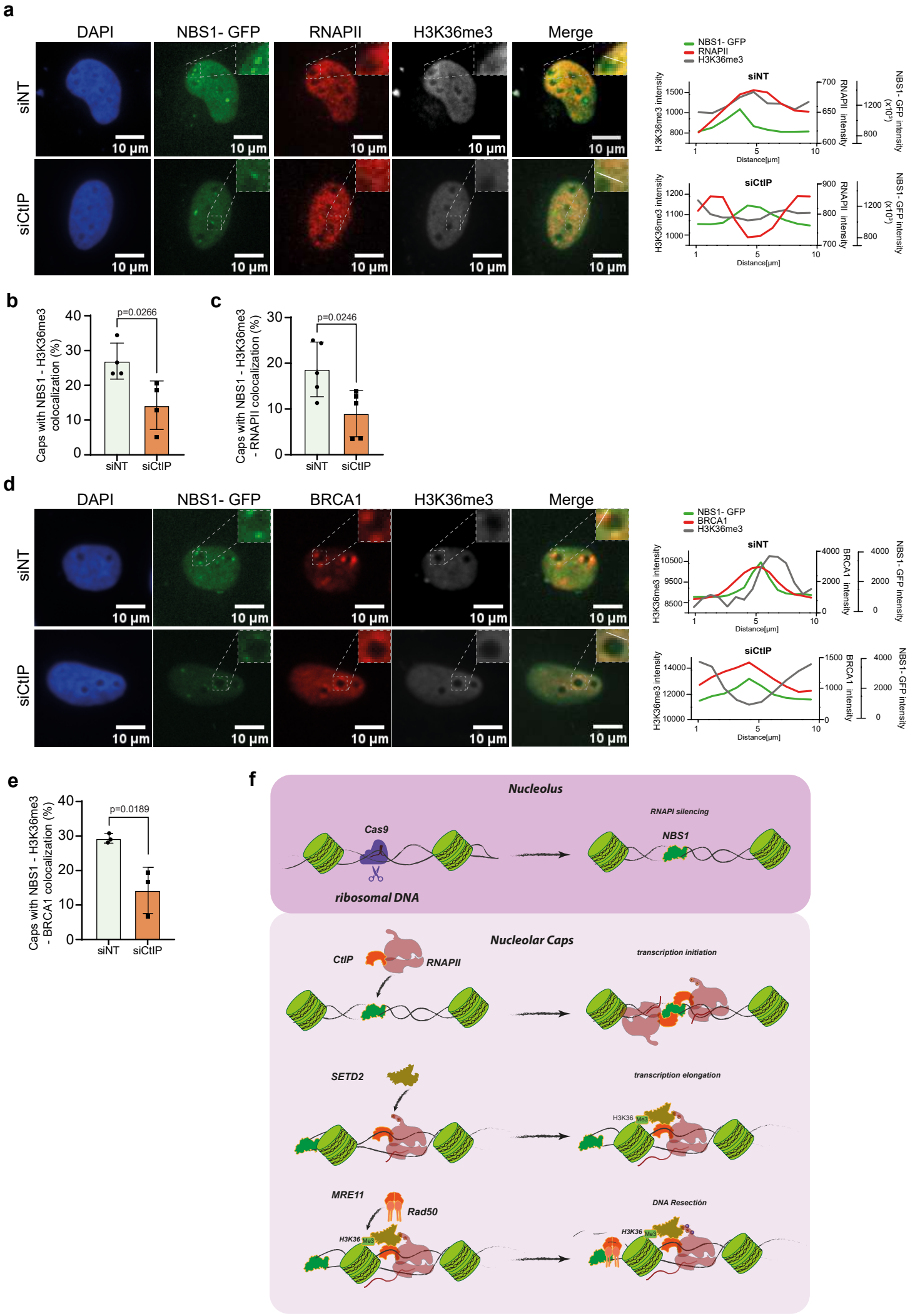

Fig. 7. Checa-Rodríguez, et al.

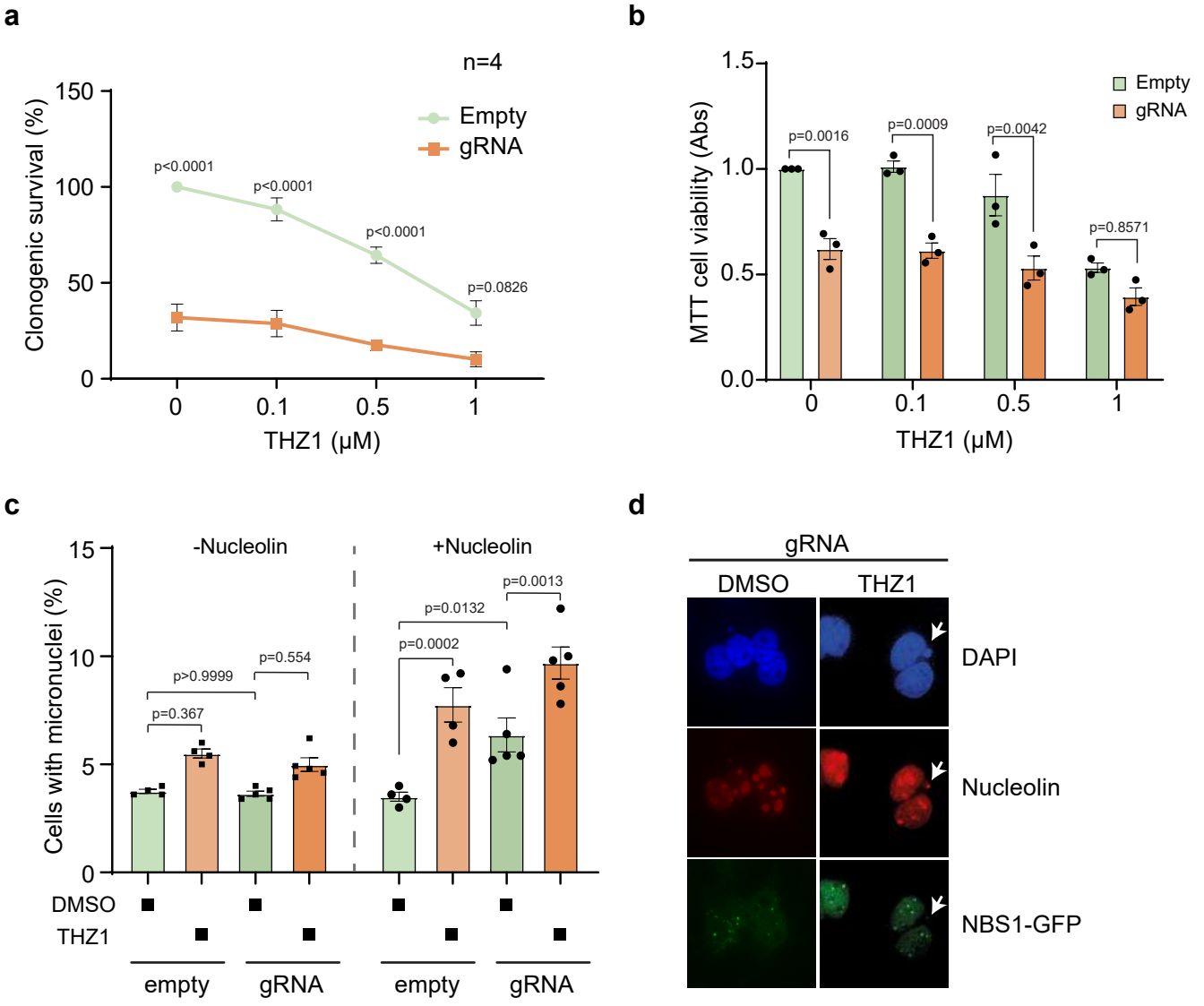

Fig. 8. Checa-Rodríguez, et al.